Compression and Reswelling of Microgel Particles after an Osmotic Shock

Jelle J. F. Sleeboom,[1,2] Panayiotis Voudouris,[1,2] Melle T. J. J. M. Punter,[3] Frank J. Aangenendt,[1,2,4] Daniel Florea,[1,2] Paul van der Schoot,[5,6] and Hans M. Wyss[1,2,4,*]

[1]*Institute for Complex Molecular Systems, Eindhoven University of Technology, 5600MB Eindhoven, The Netherlands*
[2]*Department of Mechanical Engineering, Eindhoven University of Technology, 5600MB Eindhoven, The Netherlands*
[3]*AMOLF, Theory Biomol. Matter, Science Park 104, 1098XG Amsterdam, The Netherlands*
[4]*Dutch Polymer Institute (DPI), P.O. Box 902, 5600AX Eindhoven, The Netherlands*
[5]*Department of Physics, Eindhoven University of Technology, 5600MB Eindhoven, The Netherlands*
[6]*Department of Physics, Utrecht University, 3584CC Utrecht, The Netherlands*

(Received 21 December 2016; revised manuscript received 14 June 2017; published 31 August 2017)

We use dedicated microfluidic devices to expose soft hydrogel particles to a rapid change in the externally applied osmotic pressure and observe a surprising, nonmonotonic response: After an initial rapid compression, the particle slowly reswells to approximately its original size. We theoretically account for this behavior, enabling us to extract important material properties from a single microfluidic experiment, including the compressive modulus, the gel permeability, and the diffusivity of the osmolyte inside the gel. We expect our approach to be relevant to applications such as controlled release, chromatography, and responsive materials.

DOI: 10.1103/PhysRevLett.119.098001

Microgels are microscopic polymer gels, swollen in a solvent. Because of their low internal polymer concentration, they are both mechanically soft and respond to changes in their physicochemical environment such as solvent quality, *p*H, ionic concentration, and temperature. This sensitivity to external triggers is exploited in a range of industrial and biomedical applications, where the controlled swelling or compression of these systems can, for instance, be used for the controlled release of drugs and the creation of smart, responsive materials [1].

Microgel particles or other soft objects such as biological cells generally adapt their volume under the influence of an applied osmotic pressure. This effect is often employed as a means to characterize their bulk elastic properties [2–6] by measuring the pressure-dependent compression. However, any potentially slow kinetics associated with the compression process itself is generally ignored. One reason for this is that the process of swelling and compression of these particles is usually faster than the experimental time scale required to bring about a well-defined change in the applied osmotic pressure. Hence, it is difficult to quantify the kinetics of this process in direct experiments. However, experimental access to the kinetics of such compression processes would yield valuable additional information on the viscoelastic properties of these materials that cannot be obtained by only studying the particle properties under (quasi-) equilibrium conditions.

In this Letter, we study these effects experimentally on a model system of microgel particles. To apply a rapid and well-controlled osmotic shock, we use dedicated microfluidic devices that enable us to subject microgel particles to rapid changes in osmotic pressure, while simultaneously visualizing the time-dependent changes in particle size by video microscopy. We observe a surprising nonmonotonic response, where an initial rapid compression is followed by a slow reswelling of the particles, during which they approximately regain their original size. The former we attribute to a poroelastic compression under constant external pressure, while the latter must be due to a penetration of the osmolyte into the microgel network, which in turn leads to a reduction of the osmotic pressure difference between the inside and outside of the microgel particles.

We perform our experiments on a model system of polyacrylamide (PAA) microgel particles, synthesized by polymerization of aqueous drops in a water-in-oil emulsion. The aqueous phase contains all the reagents for the polymerization of PAA, acrylamide monomers, sodium chloride, as well as the cross-linker BIS-acrylamide. We synthesize three different batches: "soft," "medium," and "stiff" particles. For the soft and medium particles we use 5 wt % of acrylamide monomers, 12 wt % of sodium chloride, and respectively 0.1 and 0.5 wt % of BIS-acrylamide in the aqueous phase. We then allow the polymerization reaction to take place inside the aqueous droplets by keeping the emulsion at a temperature of 65 °C for ∼10 h, resulting in the formation of a cross-linked polymer network inside the droplets. For the stiff particles we use a microfluidic device to make aqueous droplets which contain 10 wt % of acrylamide monomers, 0.26 wt % BIS-acrylamide, and 0.1 wt % of the catalyst ammonium persulfate. The outer phase contains 0.1 wt % of the initiator tetramethylethylendiamin (TEMED). After polymerization, all our PAA particles are subjected to a series of

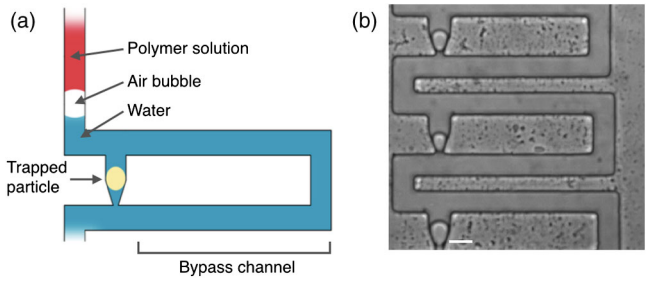

FIG. 1. Microfluidic particle trapping device for osmotic shock measurements. (a) Schematic of a single trap. (b) Typical device, showing trapped particles; scale bar is 40 μm.

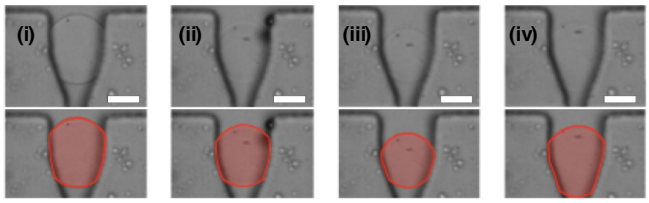

FIG. 2. Typical osmotic shock experiment on a medium particle. Microscope images showing a trapped particle, prior to the shock (i), at $t \approx 4$ s (ii), near the minimum volume at $t \approx 10$ s (iii), and at $t \approx 100$ s (iv). Scale bar is 20 μm. Particle outline highlighted for clarity in lower row of images.

washing steps, where the oil phase and any remaining unreacted monomers are removed by centrifugation, removal of supernatant, and dilution with deionized water (MilliQ, resistivity $\sigma > 18$ MΩ cm).

Our microfluidic devices are fabricated from polydimethylsiloxane (PDMS) using standard soft lithography techniques [7]. They incorporate microfluidic particle traps similar to those described by Tan *et al.* [8], with an operation principle shown schematically in Fig. 1(a). When particles initially enter the device, they flow into empty traps because the fluid resistivity of the trap is lower than that of the bypass channel. After a particle is caught in a trap, the situation is reversed and subsequent particles pass through the bypass channel. In a typical osmotic shock experiment, we first flow water past the particles, followed by a fluid of higher osmotic pressure, separated by an air bubble to avoid any diffusion- or convection-induced smoothing of the interface between the two fluids.

During this process, we record the time-dependent changes in particle size by video microscopy. Representative frames are shown in Fig. 2 for a typical experiment on our medium microgel particles exposed to an osmotic shock from zero to 29.4 kPa using a 13 wt % dextran solution ($M_r = 70$ kg/mol, Sigma-Aldrich, Cat. No. 31390). The bottom of Fig. 2 shows particle outlines for clarity. For each frame of the corresponding movies, we estimate the particle volume $V(t)$ using digital image analysis (see Supplemental Material [9]).

We generally observe that the particles respond initially by shrinking relatively swiftly after which they slowly reswell to approximately their original size, as shown in Fig. 3(a). The volume of the particle immediately after it is exposed to the high osmotic pressure remains unchanged, showing that the transfer of the bubble, as well as the exchange to a fluid of higher viscosity, has no significant impact. Instead, the subsequent compression of the particle must be caused solely by the increase in osmotic pressure. We confirm this by performing experiments at different flow rates, 500 and 1000 μL, finding no discernible differences [9]. We thus perform all subsequent experiments at 1000 μL/h, and vary only the osmotic pressure, as well as the particle stiffness. The latter should dictate the elastic response of the particles and the transport of osmolyte into the particles. Through the former, we control the level of external stress applied to the particle. We find that increasing the osmotic pressure leads to a larger level

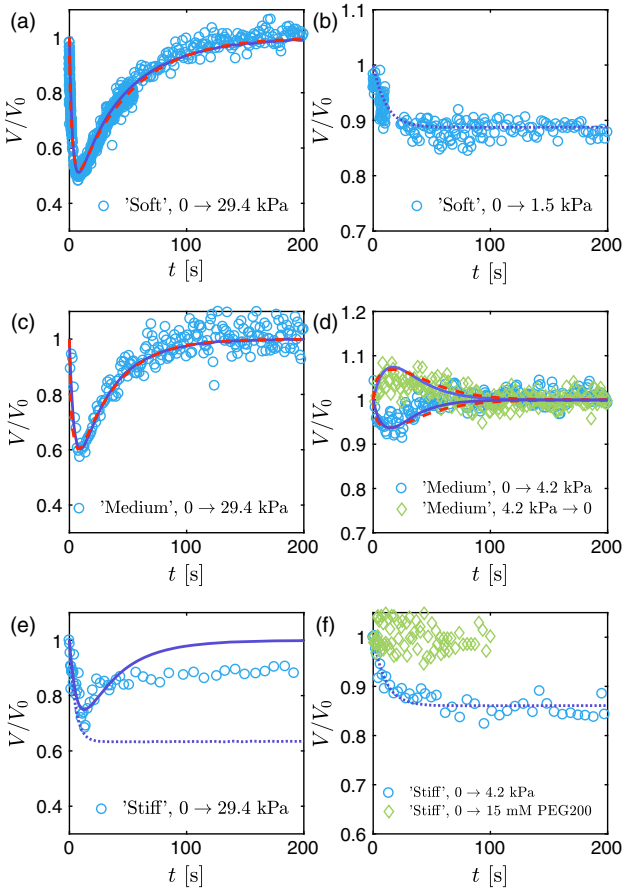

FIG. 3. Experimental data and model fits for different conditions, as indicated in each subfigure. A high molecular weight (2 MDa) poly-ethyleneglycol (PEG) osmolyte is used in (b) and a low molecular weight (200 Da) PEG in the top curve of (f). All other experiments use 70 kDa dextran as an osmolyte. Fits to the phenomenological model are shown as a blue solid or blue dotted line for cases where the osmolyte can or cannot enter the gel, respectively. Fits to the poroelastic continuum model are shown as a red dashed line.

of compression, while increasing the particle stiffness leads to a lower compression, but a somewhat faster recoiling, as shown in Figs. 3(a), 3(c), and 3(e).

In our hypothesis of the physical origin of the observed behavior, the slow reswelling process is governed by a penetration of osmolyte into the pores of the microgel. A simple way to test this hypothesis is to use an osmolyte that is larger than the pores of the network and thus cannot readily penetrate the polymer particle. Indeed, as shown in Fig. 3(b), using a high molecular weight polyethylene oxide solution ($M_w = 10^6$ g/mol, 2 wt %) to induce the osmotic shock, we observe only a rapid compression without any signs of reswelling, thus confirming our hypothesis. We observe similar effects when decreasing the mesh size of the hydrogel. For our stiff particles, an osmotic shock with a 5 wt % 70 kDa dextran ($\Pi \approx 4.2$ kPa) leads to a rapid compression without reswelling, consistent with a modulus of $K \approx 18$ kPa, as shown in Fig. 3(f). When applying a higher osmotic pressure (13 wt % 70 kDa dextran, $\Pi \approx 29.4$ kPa) we do observe some reswelling, but the particle does not regain its initial size, as shown in Fig. 3(e). Partitioning of the osmolyte between the inside of the particle and its surroundings thus appears to be strongly dependent on the polymer concentration and the molecular weight, as expected [12].

We also perform experiments using osmolytes of very low molecular weight, with qualitatively different results. Using polyethylene glycol, PEG200 ($M_w = 200$ g/mol), we do not observe any significant compression, as shown in Fig. 3(f). Indeed, it is reasonable to assume that osmolytes much smaller than the mesh size can freely diffuse into the particle without interacting significantly with the gel network. This picture implies that for small enough osmolytes no significant forces are applied to the gel network and thus the volume of the gel remains unchanged. However, solvent quality effects due to the addition of osmolytes such as salt or sugars should also be taken into account (see Supplemental Material [9]).

To further rationalize our findings, we develop a model that, despite its simplicity, captures the essential physics of the response of microgel particles to an osmotic shock. We assume that an equilibrated particle of initial radius R_0 is at time $t = 0$ instantaneously exposed to a constant osmotic pressure Π, exerted by an osmolyte present in the surrounding fluid. Let the concentration of osmolyte at $t = 0$ be uniform outside of the microgel particle and zero inside. Plausibly, we assume that, due to the presence of the polymer network, diffusion of the osmolyte inside the particle is much slower than that outside the particle. Moreover, in our osmotic shock experiments, we are continuously flowing fresh osmolyte solution along the particle surface. Hence, we expect the osmolyte concentration and chemical potential at the surface to remain constant. If this is true, we only need to consider the slow diffusion process within the microgel particle itself.

Because diffusion of osmolyte into the microgel is slow, the microgel responds elastically to the osmotic pressure difference caused by different concentrations of osmolyte inside and outside the microgel. If we rely on simple relaxational dynamics [13], then a sensible ansatz for a dynamical equation describing the time evolution of the radius $R(t)$ of the particle would be $\partial R/\partial t = -\Gamma \partial \Psi/\partial R$, where Γ is a kinetic coefficient, $-\partial \Psi/\partial R$ is a generalized force, and Ψ an appropriate free energy. The kinetic coefficient describes how easily the fluid is squeezed out of the microgel if it is under a compressive force.

The free energy Ψ describes the mechanical and chemical work done during a volume change, and is a function of the elastic properties of the gel network. We simplify our description further by neglecting the spatial distribution of osmolyte within the particle, accounting only for the overall concentration within that particle. We further assume that the network consists of m cross-linked subchains, and that it can be described as a uniform phantom network, which does not interact with the osmolyte [14]. This means that in equilibrium the internal and external concentration of the osmolyte will be equal. In particular for cases where the microgel particles are virtually indistinguishable before and after the osmotic shock experiment, this seems a reasonable assumption.

The mean density of the osmolyte in the microgel, $\rho = (3N/4\pi R^3)$, depends on the number of osmolyte molecules in the microgel N and its radius R, if presumed spherical. The free energy of the network including the absorbed osmolyte can now be written as $\Psi = \frac{3}{2}k_BTm(R/R_0)^2 + \frac{3}{2}mk_BT(R_0/R)^2 + Nk_BT\log(\rho\upsilon) - Nk_BT - N\mu + \Pi 4\pi R^3/3$, where υ is a microscopic volume scale and μ the chemical potential of the osmolyte that is set by its concentration in the fluid. The first two terms describe the ideal elastic behavior of the gel, and the third accounts for mixing and translation of the osmolyte within the microgel. The last two terms appear on account of the host fluid acting as both an osmolyte *and* an osmotic pressure reservoir. If the background fluid behaves like an ideal solution, van't Hoff's law, $\Pi = \rho k_BT$, applies and we can directly express the chemical potential in terms of its osmotic pressure, $\mu = k_BT\log(\Pi\upsilon/k_BT)$.

This produces the following dynamical equation for the ratio $\alpha(t) = R(t)/R_0$ of the size of the microgel at time t relative to that at time zero, $(\partial\alpha/\partial t) = -\Gamma_\alpha[\alpha - \alpha^{-3} - P\alpha^{-1} + P\alpha^2]$, where $P \equiv \Pi/K$ is the osmotic pressure scaled by the bulk compressive modulus $K \approx mk_BT/R_0^3$ of the network, and $\Gamma_\alpha \equiv \Gamma k_BT/R_0^2$ is a relaxation rate. The appropriate initial condition is $\alpha(0) = 1$. To account for diffusion of the osmolyte from the fluid into the microgel, we invoke the diffusion equation in integral form, $\partial N/\partial t = D \oint d^2S \cdot [\rho\nabla\mu/k_BT]$ across the interface, where D is the diffusivity of the osmolyte within the gel. Within our coarse-grained model prescription in which the osmolyte behaves ideally and

where we treat the concentrations inside and outside the microgel particle as uniform but different, this becomes $\partial N/\partial t = DR^{-2}(N_\infty - N)$ with $R(t)$ the radius of the microgel and N_∞ the equilibrium value of the number of osmolyte particles; all constants of proportionality are absorbed in the diffusivity.

If we define $f(t) = N(t)/N_\infty$ as the fraction of the total equilibrium amount of osmolyte in the microgel at time t, we obtain $(\partial f/\partial t) = -\Gamma_f \alpha^{-2}(f-1)$, where we have introduced the kinetic parameter $\Gamma_f \equiv D/R_0^2$ that sets the time scale for the solute to enter the microgel by diffusion. An obvious initial condition is $f(0) = 0$. The ratio of the rates $\gamma = \Gamma_f/\Gamma_\alpha$ determines to what extent the microgel particle can be compressed if exposed to an instantaneous osmotic stress and also determines the time scale over which reswelling occurs.

The reverse case of exposing an osmolyte-saturated microgel particle to a solvent devoid of any osmolyte, produces slightly different differential equations that within our treatment read $\partial\alpha/\partial t = -\Gamma_\alpha[\alpha - \alpha^{-3} - fP]$ and $\partial f/\partial t = -\Gamma_f \alpha^{-2} f$, where P has the same meaning as before, describing the osmotic pressure of the solution before it is replaced by pure solvent, and $f(t) = N(t)/N(0)$ is the fraction of osmolyte depleted from the microgel particle. Initial conditions are $\alpha(0) = 1$ and $f(0) = 1$. In this case the particle swells immediately after immersion into pure solvent because of the osmotic pressure exerted by the osmolyte trapped within the microgel.

Inserting the formal solution to Eq. (2) into Eq. (1), produces a nonlinear integrodifferential equation that we have not been able to solve analytically. Even for small pressures $P \ll 1$, an exact solution remains elusive albeit that the short- and long-time relaxation can be evaluated. The short-time response is exponential and dominated by a relaxation rate equal to $3\Gamma_\alpha(12+3P)$, while the long-time response is biexponential with relaxation rates Γ_f and $\Gamma_\alpha(12+9P)$. This shows that the relevant time scales are functions of the diffusivity of the osmolyte within the microgel (through Γ_f), the cross-linking density and the permeability of the microgel (through Γ_α and P), the osmotic pressure of the solution (through P), as well as the size (through Γ_f, Γ_α, and P).

In the limit $P \ll 1$ an approximate solution for all times can be given. For osmotic compression and reswelling of an initially pure microgel we obtain $\alpha \approx 1 - P(4+3P-\gamma)^{-1}\{\exp(-\Gamma_f t) - \exp[-(12+9P)\Gamma_\alpha t]\}$, which is close to the experimental data and to the full numerical solution. For swelling and recompression of an osmolyte-saturated microgel in pure solvent we get $\alpha = 1 + (P/4 - \gamma)[\exp(-\Gamma_f t) - \exp(-12\Gamma_\alpha t)]$. This highlights that the compression and swelling experiments are not symmetric due to their inherently nonlinear character.

We have also developed a more detailed model, based on conventional poroelastic theory, [15] in which we take into account the local force balance between osmotic pressure of the dissolved polymers, and the mechanical response of the network. To compare this model to our phenomenological model it assumes the dextran inside the hydrogel to be unhindered by the PAA network; i.e., we consider again the PAA network as a phantom network. The full geometric nonlinearity of large deformations is captured by assuming Hencky elasticity for the effective stress [15]. Interaction between the PAA network and water is modeled with Darcy's law [16]. More details can be found in the Supplemental Material [9] and will be discussed extensively in a follow-up article. We evaluate numerically the governing equations for both models, optimizing the various model parameters against the experimental data. As shown in Fig. 3, this yields a surprisingly good agreement between both models and the experimentally observed compression and swelling curves. In Table I we collect the fitted model parameters corresponding to the experiments shown in Fig. 3. We can relate the model parameters obtained from these fits to more intuitive material properties such as the water permeability of the gel network κ, the bulk compressive modulus of the network K, and the diffusion coefficient of the osmolyte in the network D.

TABLE I. Parameters and corresponding material properties for the model curve fits displayed in Fig. 3. Input parameters are the particle radius, $R \approx 20$ μm, and the Poisson ratio, $\nu = 0.48$. The time scales for the phenomenological model are $t_{\text{fast}} = \pi^2[3\Gamma_\alpha(12+3P)]^{-1}$, $t_{\text{slow}} = \pi^2/\Gamma_f$.

	Soft		Medium			Stiff		
Data in Figures:	3A	3B	3C	3D	3D	3E	3E	3F
Π [kPa]	29.4	1.5	29.4	4.2	−4.2	29.4	29.4	4.2
Parameters phenomenological model:								
K [kPa]	10	10	13	13	13	30	30	18
t_{fast} [s]	19	43	32	61	72	33	26	42
t_{slow} [s]	493	⋯	395	132	132	329	⋯	⋯
D [μm^2/s]	0.81	⋯	1.01	3.04	3.04	1.22	⋯	⋯
κ [nm^2]	2.11	0.93	0.98	0.51	0.43	0.40	0.50	0.53
Parameters poro-elastic model:								
K [kPa]	11	⋯	14	14	14	⋯	⋯	⋯
t_{gel} [s]	53	⋯	60	60	60	⋯	⋯	⋯
t_{pol} [s]	350	⋯	240	240	240	⋯	⋯	⋯
D [μm^2/s]	1.1	⋯	1.7	1.7	1.7	⋯	⋯	⋯
κ [nm^2]	0.23	⋯	0.16	0.16	0.16	⋯	⋯	⋯

We obtain K directly from the fitted value of $P \equiv \Pi/K$, and D we obtain from $\Gamma_f = DR_0^2$. For our medium particles the obtained modulus $K \approx 13$ kPa is in good agreement with the $K \approx 13 \pm 5$ kPa that we obtained from an independent Capillary Micromechanics measurement [17,18] (see the Supplemental Material [9]). For our stiff particles, Capillary Micromechanics yields $K \approx 33.5 \pm 11$ and $K \approx 17.8 \pm 6$ kPa for the high-strain and low-strain regime, respectively [9]. This compares favorably with the values of

$K = 30$ and $K = 18$ kPa corresponding to the model curves in Figs. 3(e) and 3(f).

To obtain the permeability κ, we identify the kinetic coefficient Γ_α with the fast relaxation process in the swelling process, described by the analytical model of Tanaka and Fillmore [19] as $3\Gamma_\alpha(12 + 3P) \approx \pi^2 K\kappa/R_0^2\eta$, with η the viscosity of water. Measurement of the permeability usually requires dedicated setups such as the flow cell used by Tokita and Tanaka [20] or an approach based on indentation, recently developed by Hu *et al.* [21]. While these methods do not enable direct measurements on microscopic particles, the values we obtain for the gel's permeability are of the same order as previous measurements on macroscopic PAA gels, which found $\kappa \approx 0.3$–6 nm^{-2} for polymer concentrations of $c \approx 3$–20 wt% [20]. Given the relatively weak trends in the obtained permeability values we cannot make strong statements regarding the dependence of the permeability on the applied osmotic pressure or the particle stiffness. Further, while we did not find literature data for the diffusion coefficient of dextran in PAA gels, the obtained diffusion coefficient of $D \approx 1$ μm^2/s for 70 kg/mol dextran within the PAA networks is indeed much lower than in water, where $D \approx 30$ μm^2/s [22].

In summary, our method enables direct experimental access to three key physical properties of porous soft objects: their elastic bulk modulus, their permeability to an aqueous background liquid, and the mobility of the osmolyte, the macromolecules used to apply the osmotic pressure, within the pores of the soft object. While at the macroscopic scale, measurement of each of these properties requires separate, dedicated techniques and instruments, using our microfluidic approach they become readily accessible in one simple experiment.

We expect our approach to be directly applicable to applications and materials where the properties of soft, compressible objects are of key importance.

The work of F. J. A. and H. M. W. forms part of the research programme of the Dutch Polymer Institute (DPI), project 738; we are grateful for their financial support. The work of M. T. J. J. M. P. is part of the Industrial Partnership Programme Hybrid Soft Materials that is carried out under an agreement between Unilever R&D B. V. and the Netherlands Organisation for Scientific Research (NWO).

J. J. F. S. and P. V. contributed equally to this work.

*H.M.Wyss@tue.nl

[1] L. R. B. Kesselman, S. Shinwary, P. R. Selvaganapathy, and T. Hoare, Small **8**, 1092 (2012).
[2] J. Bastide, S. Candau, and L. Leibler, Macromolecules **14**, 719 (1981).
[3] Y. Li and T. Tanaka, J. Chem. Phys. **92**, 1365 (1990).
[4] J. J. Liétor-Santos, B. Sierra-Martín, and A. Fernández-Nieves, Phys. Rev. E **84**, 060402 (2011).
[5] C. Bonnet-Gonnet, L. Belloni, and B. Cabane, Langmuir **10**, 4012 (1994).
[6] W. J. Polacheck, R. Li, S. G. M. Uzel, and R. D. Kamm, Lab Chip **13**, 2252 (2013).
[7] Y. N. Xia and G. M. Whitesides, Angew. Chem., Int. Ed. **37**, 550 (1998).
[8] W. H. Tan and S. Takeuchi, Proc. Natl. Acad. Sci. U.S.A. **104**, 1146 (2007).
[9] See Supplemental Material at http://link.aps.org/supplemental/10.1103/PhysRevLett.119.098001, which includes Refs. [10,11], for a supplemental video, a brief description of the poroelastic continuum model, as well as additional information on Capillary Micromechanics measurements, characterization of osmotic pressure, image analysis, and osmotic shock measurements using sorbitol solutions.
[10] V. Klika, Crit. Rev. Solid State Mater. Sci. **39**, 154 (2014).
[11] O. Coussy, *Poromechanics* (John Wiley & Sons Ltd., New York, 2004).
[12] J. Tong and J. L. Anderson, Biophys. J. **70**, 1505 (1996).
[13] N. Goldenfeld, *Lectures on Phase Transitions and the Renormalization Group* (Addison-Wesley, Reading, MA, 1992).
[14] A. Y. Grosberg and A. R. Khokhlov, *Statistical Physics of Macromolecules* (AIP, New York, NY, 1994).
[15] C. W. MacMinn, E. R. Dufresne, and J. S. Wettlaufer, Phys. Rev. Applied **5**, 044020 (2016).
[16] A. M. Tartakovsky, D. M. Tartakovsky, and P. Meakin, Phys. Rev. Lett. **101**, 044502 (2008).
[17] H. M. Wyss, T. Franke, E. Mele, and D. A. Weitz, Soft Matter **6**, 4550 (2010).
[18] M. Guo and H. M. Wyss, Macromol. Mater. Eng. **296**, 223 (2011).
[19] T. Tanaka and D. J. Fillmore, J. Chem. Phys. **70**, 1214 (1979).
[20] M. Tokita and T. Tanaka, J. Chem. Phys. **95**, 4613 (1991).
[21] Y. Hu, X. Zhao, J. J. Vlassak, and Z. Suo, Appl. Phys. Lett. **96**, 121904 (2010).
[22] N. P. Periasamy and A. V. Verkman, Biophys. J. **75**, 557 (1998).